Progress in Photovoltaics: Research and Applications

WILEY

PROGRESS IN PHOTOVOLTAICS

SPECIAL ISSUE ARTICLE OPEN ACCESS

Mitigation of UV-Induced Degradation in Lightweight SHJ Solar Modules via a UV-Downshifting Encapsulation Strategy

Kai Zhang[1,2] | Rongda Zhang[1,3] | Andreas Lambertz[1] | Bittkau Karsten[1] | Henrike Gattermann[1] | Uwe Rau[1,2] | Kaining Ding[1]

[1]IMD-3 Photovoltaics, Forschungszentrum Jülich GmbH, Jülich, Germany | [2]Jülich Aachen Research Alliance (JARA-Energy) and Faculty of Electrical Engineering and Information Technology, RWTH Aachen University, Aachen, Germany | [3]Faculty of Georesources and Materials Engineering, RWTH Aachen University, Aachen, Germany

Correspondence: Kai Zhang (k.zhang@fz-juelich.de) | Kaining Ding (k.ding@fz-juelich.de)

Received: 30 June 2025 | **Revised:** 11 March 2026 | **Accepted:** 14 March 2026

Keywords: lightweight solar module | reliability | silicon heterojunction | UV-downshifting encapsulants | UV-induced degradation (UVID)

ABSTRACT

Lightweight photovoltaic (PV) applications are pivotal for expanding the adoption of solar energy, enabling new installation scenarios and contributing significantly to the renewable energy capacity. However, degradation due to ultraviolet (UV) radiation is a critical concern for silicon heterojunction (SHJ) solar modules, particularly lightweight solar module configurations, where flexible polymer-based front sheets may provide reduced shielding against UV radiation. In this study, we present a comprehensive investigation of the UV-induced degradation (UVID) behavior of lightweight SHJ solar modules utilizing encapsulants with different UV-transmission: UV-blocking, UV-transmitting, and UV-downshifting. After indoor UV exposure of 120 kWh/m^2, equivalent to 30 months of outdoor exposure in Jülich, Germany, solar modules incorporating these encapsulants exhibited relative efficiency losses of 2.17%, 9.25%, and 6.15%, respectively. The decrease in efficiency was mainly attributed to a reduction in the fill factor (*FF*) of the solar modules, accompanied by a diminished pseudo fill factor (p*FF*). Based on detailed *FF* and p*FF* loss analyses, we found that p*FF* loss was the major cause of *FF* loss, which is attributed to the deterioration of the passivation properties due to UV radiation. Additionally, the influence of series resistance (R_s)-related *FF* losses increased, which is attributed to the deterioration of the interconnection foil rather than the UV radiation itself. Additionally, while downshifting (DS) encapsulants helped mitigate UV damage, we observed a diminished DS effect in lightweight configurations, potentially due to photooxidation. Utilization efficiency of DS decreases from around 34% to 21% after 120 kWh/m^2 of UV exposure. Therefore, a novel encapsulation architecture combining UV-downshifting and UV-blocking encapsulants was proposed to ensure the UV utilization and stability of lightweight SHJ solar modules. Solar modules featuring this innovative dual-layer structure preserved over 98% of their initial performance after UV exposure, demonstrating a promising new approach for enhancing UV stability. The comprehensive investigation provides substantial insights into the degradation mechanism of lightweight SHJ solar modules under UV exposure and offers practical strategies in the progress of improving their durability and performance.

1 | Introduction

The growing global demand for advanced high-efficiency photovoltaic (PV) technologies has led to extensive research into silicon heterojunction (SHJ) solar cells and modules, owing to their superior power conversion efficiency, bifacial structure, low temperature process, and excellent temperature coefficient [1–7]. The world record efficiency of 27.08% for both

sides contacted SHJ solar cell was achieved by Trinasolar in December 2024 [8]. Among the strategies to further enhance the application scenarios of SHJ solar modules, the use of lightweight designs coupled with advanced encapsulation materials has gained increasing attention [9, 10]. Lightweight solar modules are not only applicable to ground installations but also open up scenarios such as vehicle-integrated PV (VIPV).

The concept of the lightweight solar module is to replace the conventional glass cover with a polymeric sheet [10–14], thus resulting in a different microenvironment as compared to traditional glass/back sheet solar modules. Therefore, there are higher requirements for the encapsulation of lightweight solar modules to ensure their long-term stability and reliability.

UV-induced degradation (UVID) has been identified as one of the most critical reliability issues for SHJ solar cells and modules. This poses a serious concern when SHJ solar modules are operating in the field, particularly for lightweight solar module configurations, where flexible polymer-based front sheets may provide reduced shielding against ultraviolet (UV) radiation. Previous studies have reported that SHJ solar modules exhibit an average yearly degradation rate of 0.7% in the field, mainly related to failures caused by encapsulant discoloration, loss of passivation, moisture ingress, corrosion of TCO layers [15], potential-induced degradation (PID), and UV radiation [16]. A study systematically examined the UVID phenomenon in SHJ solar cells alongside other advanced crystalline silicon (c-Si) PV technologies. The findings revealed that SHJ solar cells were particularly sensitive to UV radiation, exhibiting substantial power losses of up to 11.8%, which was significantly higher than the conventional aluminum back surface field (Al-BSF) solar cells with power loss typically below 1% [17]. Furthermore, it was found that the efficiency degradation due to UV radiation was primarily a result of a decrease in open-circuit voltage (V_{oc}) and fill factor (*FF*). Further research found that UVA photons, with a wavelength of 365 nm or lower, have the capacity to break silicon–hydrogen (Si–H) bonds (bond dissociation energy of ~3.4 eV corresponding to ~365 nm), increasing the dangling bond dissociation on the silicon surface, thus leading to a reduction in the chemical passivation of SHJ solar cells, resulting in increased surface recombination [18–20]. This process can significantly reduce the hydrogen content in both intrinsic (<i>a-Si:H) and doped hydrogenated amorphous silicon (a-Si:H) films, thus leading to the degradation of the interface passivation layer, resulting in a decrease in V_{oc}. Sinha et al. confirmed that the UVID of SHJ solar cells is ascribed to the loss of hydrogen (H) near the intrinsic hydrogenated amorphous silicon and crystalline silicon (<i>a-Si:H/c-Si) interface or in <i>a-Si:H layer, resulting in poor <i>a-Si:H/c-Si interface passivation [17]. In addition, many studies have revealed that UV radiation not only causes UVID of solar cells but also deteriorates polymer encapsulation materials [21–25]. UV radiation can trigger chemical reactions and degradation processes of polymers in solar modules, which changes the primary structure of the polymer, causing cross-linking or breaking of the chains, and other chemistry alterations [23]. Typical defects, such as encapsulant discoloration (e.g., [ethylene-vinyl acetate: EVA] yellowing), are caused by photooxidation due to UV radiation, thereby decreasing its transmittance [23, 26–28]. UV radiation will also lead to the degradation of the back sheet, resulting in reliability issues such as powdering and embrittlement [21, 29]. Therefore, the adoption of encapsulants with UV-blocking properties was used as one strategy to effectively mitigate the degradation of solar cells and materials induced by UV radiation, thereby ensuring the long-term stability of solar cells and modules.

In recent years, with the development of the advanced c-Si solar cell technology, like SHJ and Tunnel Oxide Passivated Contact (TOPCon) solar cells [30, 31], the requirement of the maximum utilization of the short-wavelength response is increasing. Advanced solar cells have an optimized spectrum response in the short-wavelength range; however, they are typically more sensitive to UV radiation than Al-BSF and passivated emitter rear contact (PERC) solar cells [32]. Therefore, the implementation of UV-blocking encapsulants in SHJ and TOPCon solar modules is no longer a good option, as this will certainly diminish their advantages in short-wavelength response and come at the cost of a reduced short-circuit current (I_{sc}). The other option is to use UV-transmitting encapsulants for advanced c-Si solar cell technology to better utilize the photogenerated current in the short-wavelength range, thus improving the efficiency of the solar modules. However, these advanced c-Si solar cells are susceptible to UVID [33]. To address these issues, it has been found that incorporating UV-downshifting encapsulants into solar modules is a more suitable solution [34–37]. UV-downshifting encapsulants, which are able to shift high-energy UV photons to visible light, offer promising benefits for both energy yield improvement and material protection. Firstly, the solar cell can use the shifted photons more effectively due to its higher external quantum efficiency (*EQE*) in the specific shifted wavelength range compared to the *EQE* of the UV wavelength range from which the photons were shifted. This improves the efficiency of the solar module. Secondly, most of the high-energy UV photons are shifted, preventing the UV photons from reaching the solar cells, thus diminishing the UVID. However, despite the promising potential of UV-downshifting encapsulants, the long-term reliability of lightweight SHJ solar modules incorporating UV-downshifting encapsulants remains insufficiently understood, particularly under prolonged UV exposure.

This study aims to investigate the mechanisms of UVID in lightweight SHJ solar modules utilizing encapsulants with different UV-transmission properties, involving UV-blocking, UV-transmitting, and UV-downshifting encapsulants. By systematically analyzing the changes in optical and optoelectronic properties under accelerated UV exposure of 120 kWh/m^2, this work seeks to provide a comprehensive understanding of the degradation pathways and thus proposes an innovative encapsulation strategy for reliability enhancement in next-generation SHJ solar modules.

2 | Experiment and Method

2.1 | Solar Module Design

Figure 1 shows the schematic cross section of the single-cell lightweight SHJ solar module. M2 (156.75 × 156.75 mm) 0-busbar (0BB) and M2-half-cut (156.75 × 78.37 mm) 9-busbar (9BB) bifacial monocrystalline *n*-type rear-junction SHJ solar cells were used for solar module fabrication. The solar cells are connected

using multiwire interconnection foil, denoted as IF in the following, which is composed of 18 coated copper wires with polyethylene (PE) as a carrier foil. An electrically conductive adhesive tape (ECT) was used as an alternative to compare with IF in Section 3.1.5. Sn-Pb-coated Cu-ribbons (5 mm wide, 0.2 mm thick) were used as connectors. For solar module encapsulation, ethylene tetrafluoroethylene (ETFE) was used as the front cover material, which has a higher transmittance than glass commonly used in the PV industry (see Figure S1f). The following encapsulants were used: thermoplastic polyolefin (TPO), another TPO named PO, EVA, and downshifting-EVA (DS-EVA). These encapsulants are categorized into three groups based on their light transmission to UV light (280–400 nm). TPO and PO are UV-blocking encapsulants with different UV-blocking properties. TPO blocks the UV light under 350 nm, denoted as UV-B_{350}, while PO blocks the UV light under 375 nm, denoted as UV-B_{375}. EVA is a UV-transmitting encapsulant, denoted as UV-T. DS-EVA is a UV-downshifting encapsulant that can shift UV light to blue light, denoted as UV-DS in the following sections. Figure S2 shows the excitation and emission spectra of UV-DS encapsulant. Figure 2 shows the transmittance (T) and reflectance (R) spectra of the encapsulants. The specifications of the encapsulants are listed in Table S1. A coated polyolefin-based foil with aluminum interlayer was used as the back sheet, which is denoted as Al-bs in the following. The specifications of the front sheet and back sheet are listed in Table S2. The glass/glass and glass/back sheet module samples were used as references for comparison. Glass with a thickness of 3.2 mm was used. The edges of the solar modules were sealed using polyisobutylene (PIB) tape. Table 1 lists the configurations of the test solar modules.

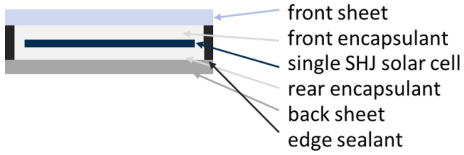

FIGURE 1 | Schematic cross section of the single-cell lightweight SHJ solar module.

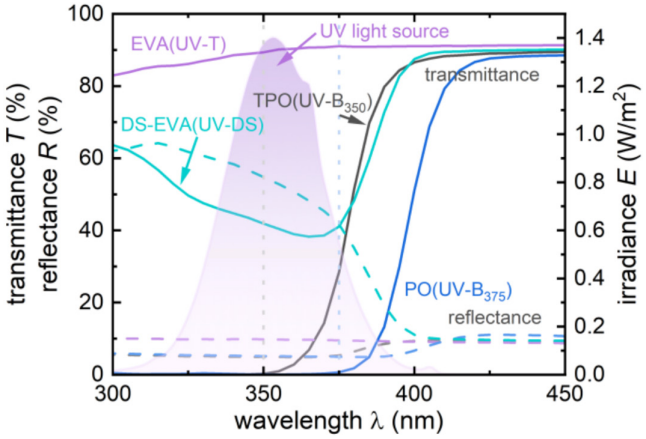

FIGURE 2 | Transmittance (solid line, T) and reflectance (dashed line, R) spectra of encapsulants with different UV-transmission properties in the range of 300–450 nm. The shaded curve shows the spectrum of the UV light source.

2.2 | Solar Module Fabrication Process

After all the foils were layered, the solar modules were fabricated by a standard vacuum lamination process using a laminator from *SM Innotech*. The maximum deviation in efficiency of all SHJ solar cells used for solar module fabrication is less than 1.50%$_{rel}$.

2.3 | UV Exposure Test

A UV exposure test was performed in a UV chamber with mercury light tubes. The UV spectrum is shown in Figure 2, with a UVA spectrum peaking at a wavelength of 353 nm. The accumulated UV intensity is approximately 56 W/m^2 integrated from 300 to 400 nm. The cumulative UV radiation dose is 120 kWh/m^2. After each 15 kWh/m^2, the solar module samples were taken out of the chamber for characterization. The temperature of the UV chamber was not controlled but was monitored by a type K Class 1 thermocouple, which was around 25°C during the UV exposure. All the solar modules were in an open-circuit condition during the UV exposure.

TABLE 1 | Configurations of the test solar modules.

Front sheet	Encapsulant (front)	Solar cell	Encapsulant (rear)	Back sheet	Interconnection
ETFE	TPO	M2 0BB	TPO	Al-bs	IF
	PO		PO		
	EVA		EVA		
	DS-EVA		DS-EVA		
	DS-EVA + TPO		TPO		
	DS-EVA + PO		PO		
Glass	DS-EVA	M2 0BB	DS-EVA	Al-bs	IF
Glass	DS-EVA	M2 0BB	DS-EVA	Glass	IF
ETFE	EVA	M2-half-cut 9BB	EVA	Al-bs	ECT

Abbreviations: 0BB, 0-busbar; 9BB, 9-busbar; Al-bs, polyolefin-based aluminum back sheet; DS-EVA, UV-downshifting EVA; ECT, electrically conductive adhesive tape; ETFE, ethylene tetrafluoroethylene; EVA, ethylene-vinyl acetate; IF, interconnection foil; PO, another thermoplastic polyolefin; TPO, thermoplastic polyolefin.

According to the data from *Deutsche Wetterdienst* (*DWD*) [38], the annual global irradiation in Aachen, Germany, is around 1050 kWh/m^2 (1991–2002). In general, an average UV fraction of 4%–5% of global irradiation is considered a reasonable assumption for locations without UV monitoring [31]. While the local climate tends to be relatively stable from year to year, significant differences can occur between regions or climatic zones. Therefore, we can assume an annual UV radiation dose of approximately 47.25 kWh/m^2 in the Jülich area, which is only 27 km from the Aachen area. In our UV exposure test, the total UV radiation dose was 120 kWh/m^2, which corresponds to approximately 30 months of field exposure.

2.4 | Characterization Techniques

The analysis of the performance and performance degradation mechanism of the solar modules due to UV radiation was performed based on the following characterization methods.

The current–voltage (*I-V*) characterization under standard test conditions (STC: AM1.5 G, 25°C, 1000 W/m^2), *EQE*, and reflectance of the solar modules were measured by using a LOANA solar cell and module analysis system from *PV-Tools*.

Photoluminescence (PL) imaging is employed as a nondestructive diagnostic technique to evaluate the quality of the material and defects in c-Si solar cells and modules. This was performed using an in-house-built setup. Solar modules are illuminated using a 90-W near-infrared laser at 808 nm, which excites electron–hole pairs within the silicon substrate. The subsequent radiative recombination of these charge carriers results in the emission of photons, which are captured using a near-infrared (NIR) InGaAs camera. Laser light reflected from the sample surface is blocked by a 1050 ± 30-nm bandpass filter located between the sample and the camera, preventing incident laser light from contributing to the measured PL intensity.

The total spectral transmittance and reflectance of encapsulation foils were measured from 300 to 1200 nm in 5-nm steps using a UV–vis–NIR spectrophotometer with an integrating sphere (*Perkin Elmer, LAMBDA 950*).

3 | Results and Discussion

3.1 | UVID Behavior of Lightweight SHJ Solar Modules With Different Encapsulants

3.1.1 | CTM Loss Analysis

Figure 3 shows the cell to module (CTM) loss of lightweight SHJ solar modules with different encapsulants, indicating that the cell to module efficiency loss is mainly attributed to the decrease in J_{sc} and increase in R_s, the latter is resulting in an *FF* reduction. The CTM η and J_{sc} losses were calculated by Equation (1).

$$CTM^{rel}_{\eta \text{ or } J_{sc}}(\%) = \left(1 - \frac{\eta \text{ or } J_{sc} \text{ of solar module}}{\eta \text{ or } J_{sc} \text{ of solar cell}}\right) \times 100 \quad (1)$$

The solar module with UV-DS encapsulant shows the lowest loss in J_{sc} from cell to module, which benefits from the UV-downshifting effect. Since UV photons could be shifted to visible light, which can be more efficiently used by SHJ solar cells. While the solar module with UV-B$_{375}$ encapsulant shows the largest J_{sc} loss from cell to module, as most of the UV photons are absorbed by the encapsulant.

3.1.2 | Optoelectronic Properties Analysis of Solar Modules

Figure 4 shows the evolution of the electrical parameters of lightweight SHJ solar modules with different encapsulants during UV exposure. The UV-T module shows the largest efficiency degradation of 9.25%$_{rel}$ after 120 kWh/m^2 of UV exposure, which is equivalent to 30 months of outdoor exposure in Jülich, Germany [39]. The relative efficiency degradation (D_η^{rel}) was defined and calculated by Equation (2), where η_{UV0} denotes the efficiency of the solar module before UV exposure, η_{UV120} denotes the efficiency of the solar module after 120 kWh/m^2 of UV exposure.

$$D_\eta^{rel}(\%) = \left(1 - \frac{\eta_{UV120}}{\eta_{UV0}}\right) \times 100 \quad (2)$$

The efficiency loss is mainly attributed to the decrease in *FF* and V_{oc}. Previous studies have revealed that reductions in V_{oc} and *FF* in SHJ solar cells are mainly caused by the deterioration of surface passivation. High-energy UV photons can break the Si–H bond used for chemical passivation [17, 18, 40], leading to the formation of additional dangling bonds on the silicon surface and, consequently, an increase in surface recombination.

From the dark *I-V* curves of the solar modules, as shown in Figure 5, we observed an obvious increase in saturation current density (J_{01}) for the UV-T module and a slight increase in J_{01} for the UV-DS module. The increase in J_{01}, which is associated with the recombination processes occurring at the surface and within the bulk of the solar cell [41, 42], is most evident in the medium- and high-voltage regions of the dark *I-V*. This behavior is consistent with our observations and suggests that the surface passivation of the SHJ solar cells in the UV-T and UV-DS modules degraded as a result of UV radiation. The reduction in V_{oc} can be explained by the increase in J_{01}, according to the relationship between V_{oc} and J_{01} [43], as expressed by Equation (3).

$$V_{oc} = \frac{kT}{q} ln\left(\frac{J_{sc}}{J_{01}} + 1\right) \quad (3)$$

The solar module with the UV-B$_{375}$ encapsulant, which absorbs most UV photons, exhibited the most stable performance with the least efficiency degradation. The UV-B$_{350}$ module showed only a slight efficiency loss. As the UV-B$_{350}$ encapsulant cannot completely block UV light, the residual UV photons that are not absorbed by the encapsulant can still reach the solar cell and cause surface passivation damage. Interestingly, the UV-DS module demonstrated improved UV stability compared to the solar module with the UV-T encapsulant; however, it still exhibited an apparent efficiency degradation of 6.15%$_{rel}$ compared to the solar module with the UV-blocking (UV-B) encapsulant. On the one

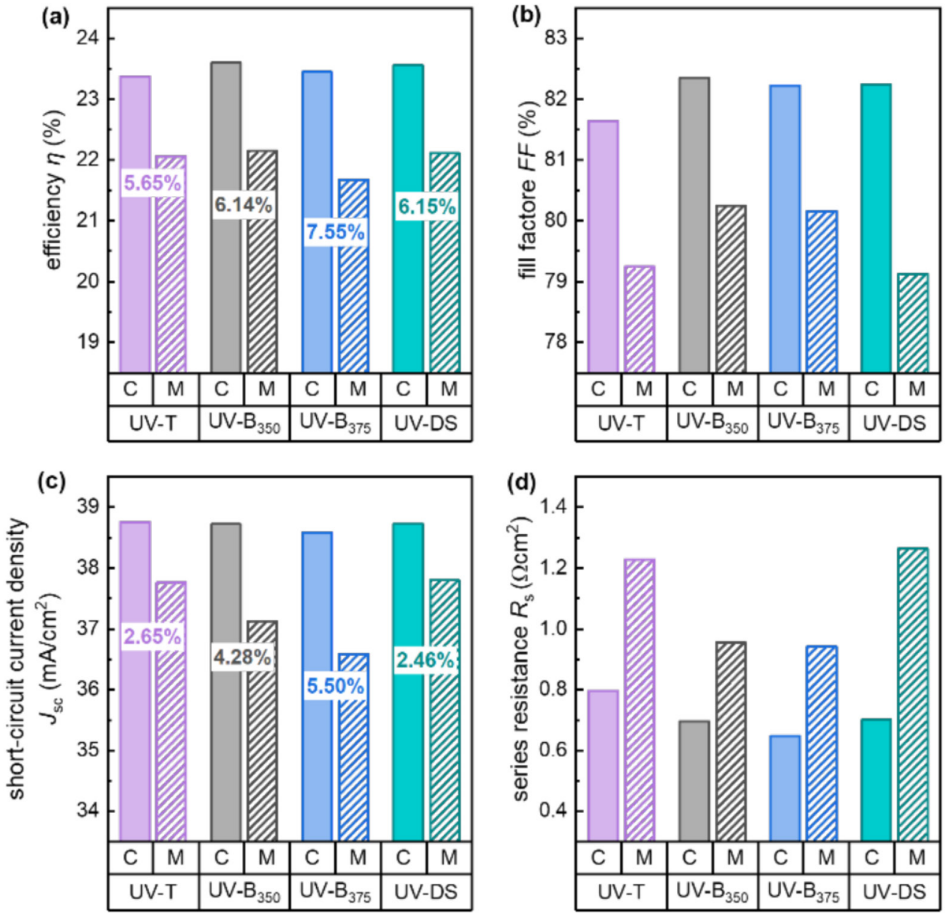

FIGURE 3 | CTM loss from (a) efficiency (η), (b) fill factor (FF), (c) short-circuit current density (J_{sc}), and (d) series resistance (R_s) of lightweight SHJ solar modules incorporating encapsulants with different UV-transmission properties. C stands for solar cell and M stands for solar module.

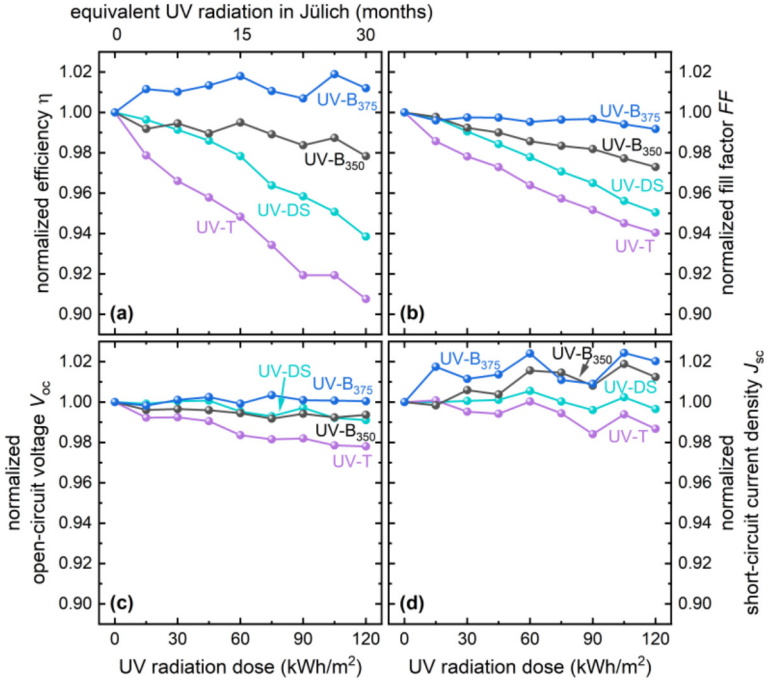

FIGURE 4 | Normalized values of (a) efficiency (η), (b) fill factor (FF), (c) open-circuit voltage (V_{oc}), and (d) short-circuit current density (J_{sc}) as a function of UV radiation dose for lightweight SHJ solar modules incorporating encapsulants with different UV-transmission properties.

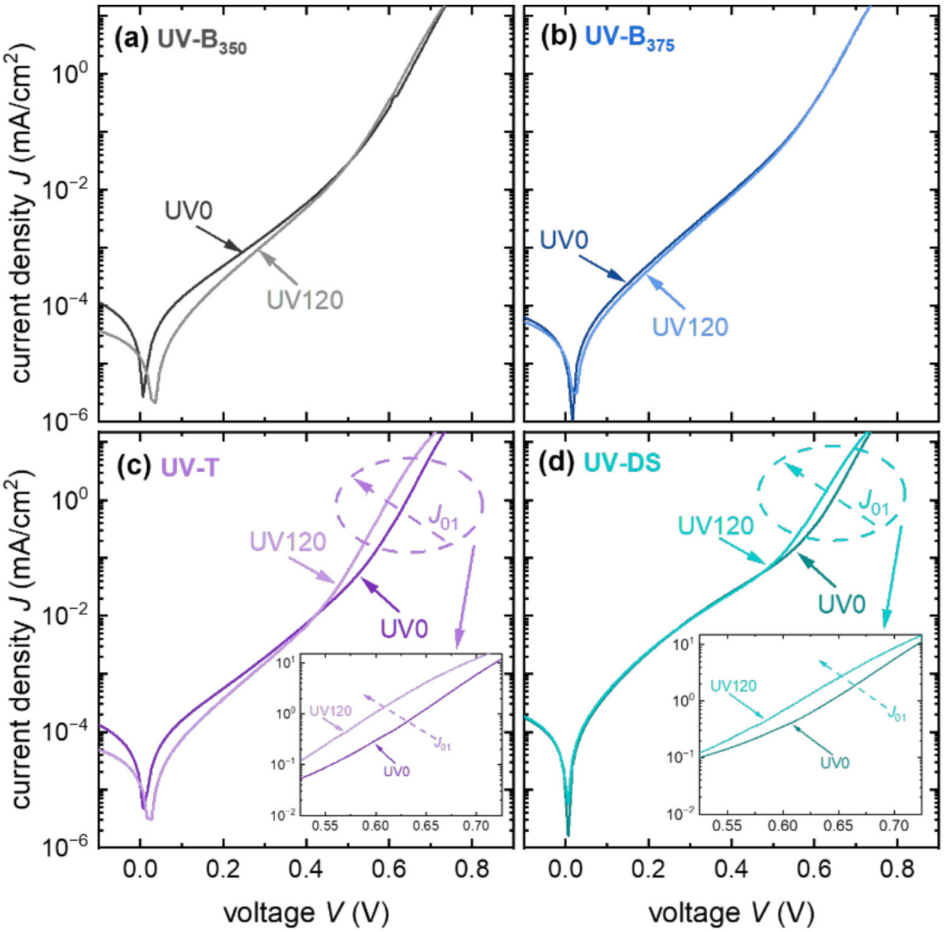

FIGURE 5 | Dark *I-V* curves of the lightweight SHJ solar modules incorporating encapsulants with different UV-transmission properties: (a) UV-B_{350}, (b) UV-B_{375}, (c) UV-T, and (d) UV-DS, measured before and after 120 kWh/m^2 of UV exposure.

hand, the UV-DS encapsulant cannot completely shift all incident UV photons into blue light; unshifted UV photons can still reach the solar cell and degrade the surface passivation. On the other hand, there is a possibility that the downshifting (DS) effect was also degraded during the UV exposure, leading to an increased fraction of UV photons that are no longer shifted to blue light. Further in-depth discussion is presented in Section 3.2.3.

To provide a direct visualization of the recombination behavior, PL imaging was performed. Figure 6 shows the PL images of lightweight SHJ solar modules with different encapsulants before and after 120 kWh/m^2 of UV exposure. A pronounced reduction in PL intensity was observed for the UV-T module. Since a large amount of UV photons can penetrate the encapsulant and arrive at the solar cell. The high-energy UV photons broke the Si–H bonds, leading to deterioration of the surface passivation and thus increased charge-carrier recombination, which in turn reduced the PL intensity. The UV-DS module exhibited moderate degradation because part of the UV photons was shifted into visible light, thereby reducing the number of UV photons reaching the solar cell and mitigating recombination losses. In contrast, the solar modules with either UV-B_{350} or UV-B_{375} encapsulant showed negligible changes in PL intensity. This is because a large fraction of UV photons was absorbed by the UV-blocking encapsulant, effectively preventing harmful UV photons from reaching the solar cell. Consequently, the passivation properties of these solar cells remained stable.

Overall, both PL intensity and V_{oc} can reflect the passivation quality of the solar cells/modules. The observed V_{oc} degradation trends are consistent with the PL imaging results, as described by Equation (4).

$$V_{oc} = V_{oc}^{ref} + \frac{kT}{q} ln\left(\frac{I_{PL}}{I_{PL}^{ref}}\right) \tag{4}$$

In addition to the efficiency loss associated with the decrease in V_{oc}, a decrease in *FF* is another major contributor to UV-induced efficiency degradation. It should be noted that *FF* losses are affected not only by carrier recombination but also by factors such as series resistance (R_s) and shunt resistance (R_{sh}). A detailed discussion of *FF* losses will be presented in the following section.

3.1.3 | *EQE* Analysis of Solar Modules

As demonstrated in Figure 7, the *EQE* and reflectance of the lightweight SHJ solar modules incorporating encapsulants with different UV-transmission properties were measured before and after 120 kWh/m^2 of UV exposure. A notable decline in *EQE*, ranging from 400 to 1000 nm, was observed in the UV-T module after UV exposure. Since the transmittance and reflectance above 400 nm of both the front sheet and the UV-T encapsulant

remained stable after UV exposure, as shown in Figure S1c,e, the *EQE* loss can be attributed to increased carrier recombination caused by passivation deterioration, rather than enhanced parasitic absorption in the encapsulation materials. This interpretation is consistent with the *I-V* and PL imaging results, where increased carrier recombination led to reductions in V_{oc}, PL intensity, and *EQE* in the 400–1000-nm range. In contrast, solar modules with UV-blocking encapsulant exhibited no measurable change in *EQE* after UV exposure.

However, the solar module with UV-DS encapsulant showed a pronounced reduction in both *EQE* and reflectance at wavelengths below 400 nm. The *EQE* decrease in this range may result from increased absorption within the UV-DS encapsulant or degradation of its DS effect. As evidenced in Figure S1d, the transmittance spectra of the UV-DS encapsulant after 120 kWh/m^2 of UV exposure showed a decrease in blue light output accompanied by an increase in transmitted UV light, providing direct proof of DS effect deterioration. Thus, the decrease in

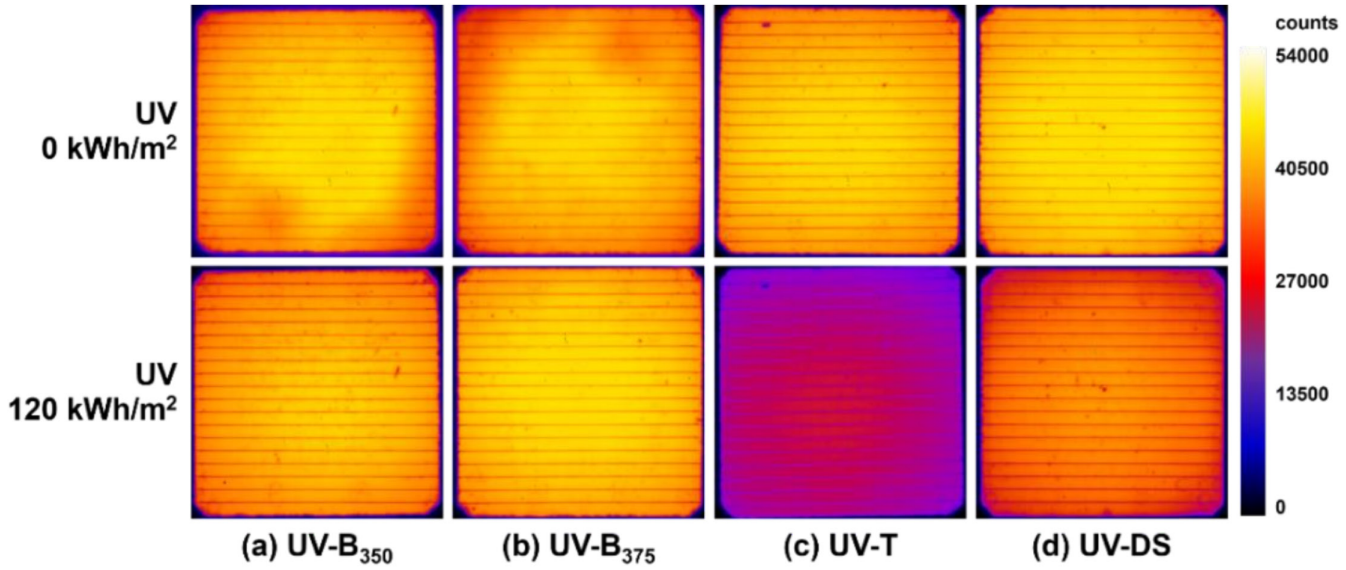

FIGURE 6 | PL images of lightweight SHJ solar modules incorporating encapsulants with different UV-transmission properties: (a) UV-B_{350}, (b) UV-B_{375}, (c) UV-T, and (d) UV-DS, before and after 120 kWh/m^2 of UV exposure.

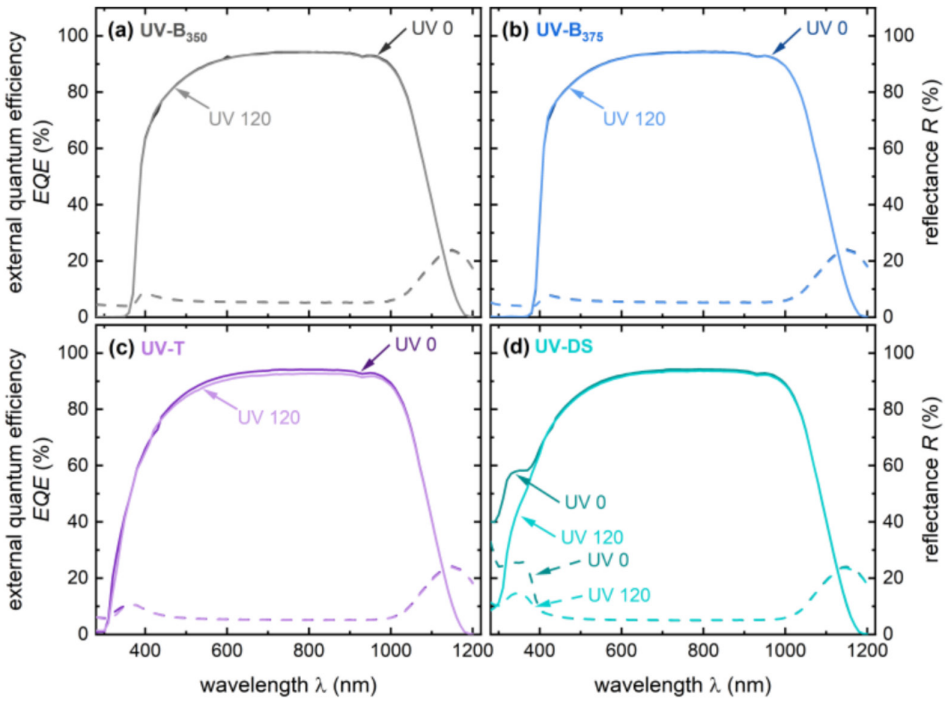

FIGURE 7 | *EQE* (solid line) and reflectance (dashed line) of lightweight SHJ solar modules incorporating encapsulants with different UV-transmission properties: (a) UV-B_{350}, (b) UV-B_{375}, (c) UV-T and (d) UV-DS, measured before and after 120 kWh/m^2 of UV exposure.

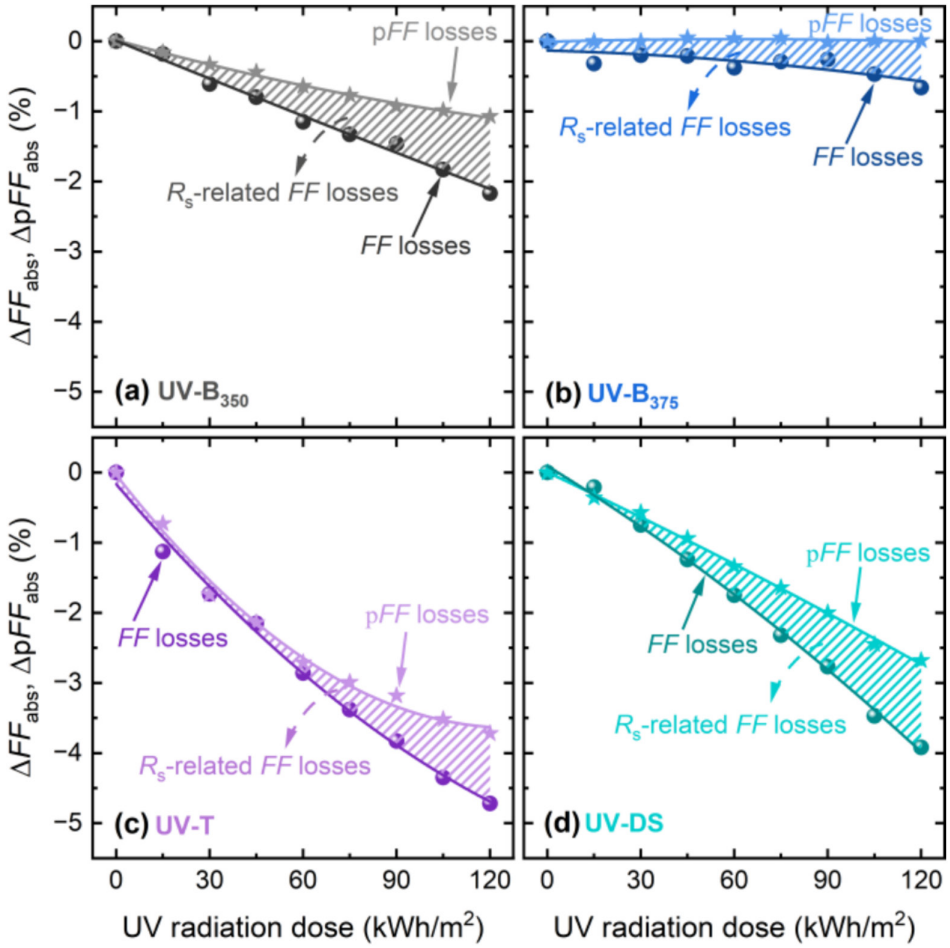

FIGURE 8 | Changes in pseudo fill factor (p*FF*) and fill factor (*FF*) of the lightweight SHJ solar modules incorporating encapsulants with different UV-transmission properties: (a) UV-B_{350}, (b) UV-B_{375}, (c) UV-T, and (d) UV-DS, as a function of UV radiation dose. ΔpFF_{abs} denotes the absolute change in p*FF*, whereas ΔFF_{abs} denotes the absolute change in *FF*.

EQE can be attributed to the degradation of the DS effect. We can therefore conclude that the DS effect was degraded due to the UV radiation in lightweight solar modules. This degradation reduces the conversion of UV photons into visible photons, allowing a greater fraction of harmful UV light to reach the solar cell. Consequently, the increased UV photons at the solar cell accelerate passivation loss, thereby lowering the overall solar module efficiency.

3.1.4 | *FF* Losses Analysis of Solar Modules

To gain further insights into the *FF* losses of the lightweight SHJ solar modules during UV exposure, the pseudo fill factor (p*FF*) of the solar modules was analyzed. The p*FF* provides a measure of *FF* without the influence of resistance losses and is a general indicator of carrier recombination in solar modules. Figure 8 shows the absolute changes in p*FF* and *FF* for lightweight SHJ solar modules incorporating encapsulants with different UV-transmission properties during UV exposure. As shown in Figure 8c,d, the *FF* losses after 120 kWh/m^2 of UV exposure were mainly attributed to p*FF* losses for the UV-T and UV-DS modules, indicating that carrier recombination was the dominant factor. Especially, the UV-T module exhibited decreases of 4.72%$_{abs}$ in *FF* and 3.72%$_{abs}$ in p*FF*, while the UV-DS module showed corresponding reductions of 3.92%$_{abs}$ and 2.68%$_{abs}$. As shown in Figure 8c, the module with UV-T encapsulant exhibited the fastest and most significant degradation in p*FF*, which correlates with its highest UV-transmittance. However, as shown in Figure 8b, the UV-B_{375} shows almost no decrease in p*FF*, indicating the UV photons were effectively blocked by the encapsulant, thus causing no measurable harm to the surface passivation of the solar cell. The slight decrease in *FF* was mainly attributed to the increased R_s-related *FF* losses. Compared to the UV-B_{375} module, the UV-B_{350} module exhibited larger *FF* and p*FF* losses, 2.17%$_{abs}$ and 1.07%$_{abs}$, respectively, with p*FF* losses and R_s-related *FF* losses contributing almost equally to the total *FF* loss.

After 120 kWh/m^2 of UV exposure, the R_s-related *FF* losses were similar across the solar modules with different encapsulants, which are 1.10%$_{abs}$, 0.67%$_{abs}$, 1.00%$_{abs}$, and 1.24%$_{abs}$ in the UV-B_{350}, UV-B_{375}, UV-T, and UV-DS modules, respectively. A previous study [40] attributed a noticeable increase in R_s-related *FF* losses in SHJ solar cells under UV exposure to elevated interface contact resistivity, rather than deterioration of the Ag electrodes or indium tin oxide (ITO) thin films. However, in our case, the similar increases observed for all solar modules incorporating different encapsulants suggest that the rise in R_s-related *FF* is not directly linked to UV-transmission properties. A more detailed analysis of this phenomenon will be provided in Sections 3.1.5 and 3.2.2.

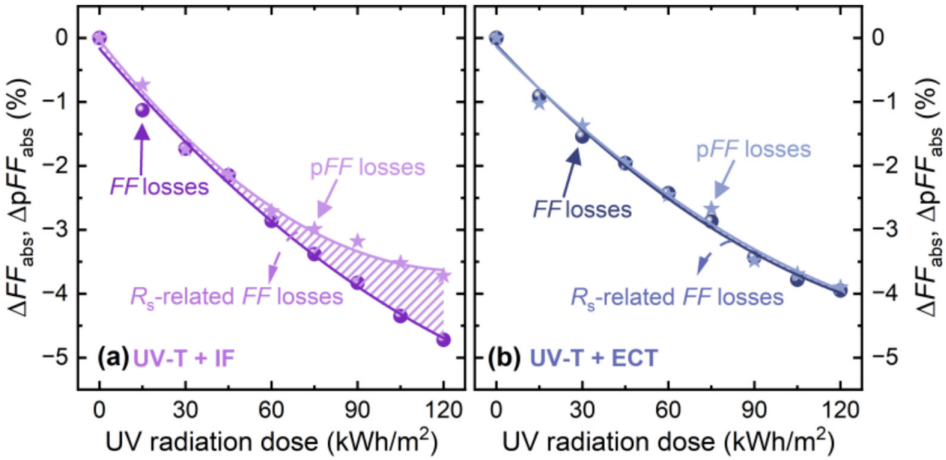

FIGURE 9 | Changes in pseudo fill factor (p*FF*) and fill factor (*FF*) of the UV-T lightweight SHJ solar modules with different interconnection methods: (a) IF and (b) ECT, as a function of UV radiation dose. ΔpFF_{abs} denotes the absolute change in p*FF*, whereas ΔFF_{abs} denotes the absolute change in *FF*.

3.1.5 | Root Causes of the Increase in R_s-Related *FF* Losses

As discussed in Section 3.1.4, R_s-related *FF* losses were similar across all encapsulant types after 120 kWh/m^2 of UV exposure, suggesting that the increase in R_s is not primarily driven by the UV-induced effect but is more likely linked to other factors. Therefore, a reasonable assumption was raised that the R_s-related *FF* losses due to the increase in R_s are due to the interconnection method. To further understand the correlation between the interconnection method and the increase in R_s, additional solar modules using the UV-T encapsulant were fabricated with ECT in place of IF and subsequently subjected to the same UV exposure protocol.

Figure 9 compares the changes in p*FF* and *FF* for solar modules with the UV-T encapsulant and interconnected using either IF or ECT. Both configurations exhibited similar overall p*FF* degradation rates. The *FF* losses of the solar module interconnected with ECT were almost entirely attributable to p*FF* losses, with a minimal increase in R_s-related *FF* losses. In contrast, the solar module with IF showed a clear increase in R_s-related *FF* losses. This suggests that the increase in R_s-related *FF* losses in lightweight SHJ solar modules stems from the interconnection foil rather than direct UV effects on the solar cells. Previous studies have reported that interconnection foils in lightweight SHJ solar modules degrade under damp heat conditions [11]. We therefore suspect that moisture ingress into the lightweight solar module may be responsible for the observed R_s increase. Further discussion is provided in Section 3.2.2.

3.2 | UVID of SHJ Solar Modules With Downshifting Encapsulants: Influence of Solar Module Structure

3.2.1 | Optoelectronic Properties Analysis of Solar Modules

Figure 10 presents the evolution of normalized electrical parameters for SHJ solar modules using UV-DS encapsulant in different solar module structures under increasing UV radiation dose. After 120 kWh/m^2 of UV exposure, the glass/glass (G/G) and glass/back sheet (G/BS) solar modules exhibited relatively low efficiency degradation of 2.18%$_{rel}$ and 1.62%$_{rel}$, respectively, compared to 6.15%$_{rel}$ of the front sheet/back sheet (FS/BS) solar module. In the G/G solar module, efficiency loss was dominated by a J_{sc} reduction of 1.32%$_{rel}$, with minimal changes in *FF* and V_{oc}. The G/BS solar module shows a similar efficiency degradation profile to the G/G solar module. By contrast, the FS/BS solar module shows the largest efficiency loss, primarily driven by declines in *FF* and V_{oc}. As shown in Figure S1f, the ETFE front sheet exhibits higher UV-transmittance than glass, allowing more high-energy UV photons to reach the solar cells, resulting in significant passivation degradation.

3.2.2 | *FF* Losses Analysis of Solar Modules

Figure 11 shows the changes in p*FF* and *FF* of the SHJ solar modules with UV-DS encapsulant in different solar module structures under increasing UV radiation dose. After 120 kWh/m^2 of UV exposure, the G/BS and G/G solar modules exhibited markedly smaller p*FF* reductions than the FS/BS solar module. Based on previous analysis, p*FF* loss is closely linked to the UVID. In the FS/BS solar modules, degradation of the DS effect allowed more UV photons to reach the solar cell, thereby increasing p*FF* loss. In contrast, the G/G and G/BS configurations effectively suppressed DS degradation, resulting in significantly lower losses.

Furthermore, R_s-related *FF* losses were negligible in the G/G solar module and only slightly increased in the G/BS solar module. As previously discussed, such losses in lightweight solar modules originate from the interconnection foil. Due to the higher water vapor transmission rates of polymer front and back sheets, lightweight designs allow for greater moisture ingress than conventional glass solar modules. The penetrated moisture can deteriorate solar cell interconnections employing interconnection foil, thereby increasing R_s-related *FF* losses [11]. We therefore speculate that the increase in R_s-related *FF* losses is due to degradation of the interconnection foil caused

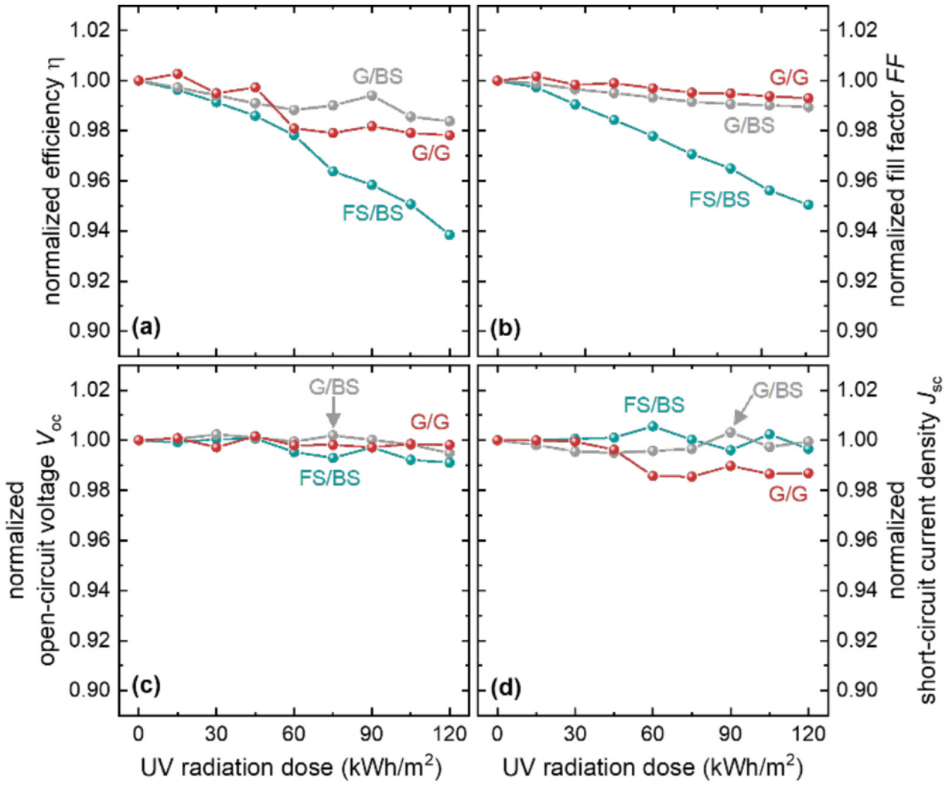

FIGURE 10 | Normalized values of (a) efficiency (η), (b) fill factor (FF), (c) open-circuit voltage (V_{oc}), and (d) short-circuit current density (J_{sc}) as a function of UV radiation dose for solar modules with UV-DS encapsulant in different solar module structures: front sheet/back sheet (FS/BS), glass/back sheet (G/BS), and glass/glass (G/G) solar modules.

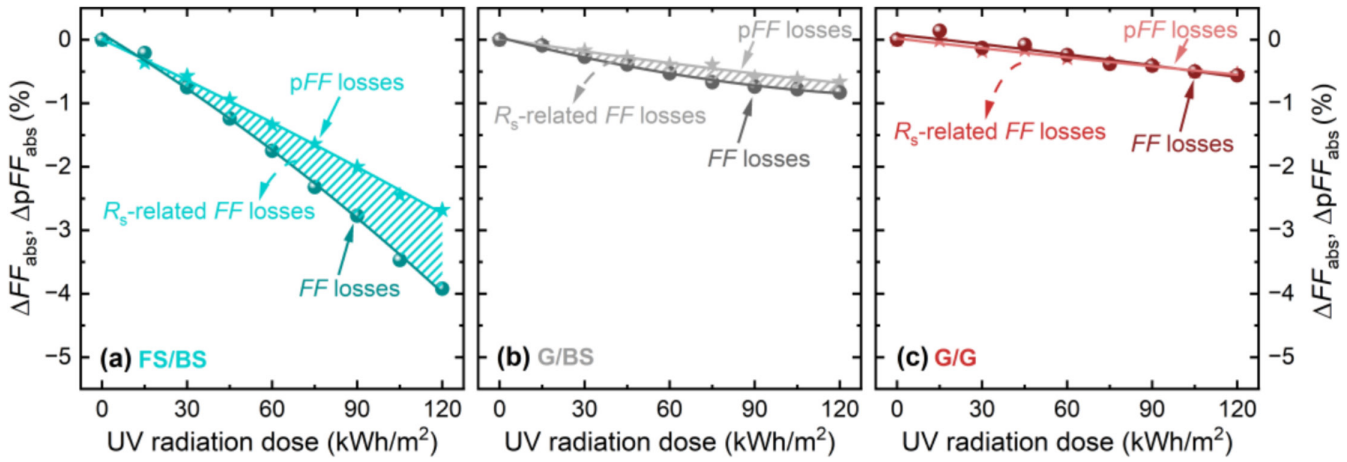

FIGURE 11 | Changes in pseudo fill factor (pFF) and fill factor (FF) of solar modules with UV-DS encapsulant in different solar module structures: (a) front sheet/back sheet (FS/BS), (b) glass/back sheet (G/BS), and (c) glass/glass (G/G), as a function of UV radiation dose. ΔpFF_{abs} denotes the absolute change in pFF, whereas ΔFF_{abs} denotes the absolute change in FF.

by moisture ingress. A thorough investigation of this issue is beyond the scope of this study, but will be explored further in subsequent work.

3.2.3 | *EQE* Analysis of Solar Modules

Figure 12 compares the *EQE* and reflectance of the UV-DS module with different solar module structures before and after 120 kWh/m^2 of UV exposure. In the FS/BS solar module, both *EQE* and reflectance dropped markedly at wavelengths below 400 nm, whereas the G/G and G/BS solar modules showed no observable changes. These results confirm that the DS effect degraded in the FS/BS configuration but remained stable in G/G and G/BS solar modules. Previous studies have shown that the synergistic action of UV photons and oxygen can trigger photooxidation, leading to polymer encapsulants degradation [21, 28, 44]. It is therefore reasonable to attribute the deterioration of the downshifting particles in FS/BS solar modules to photooxidation. Compared with a glass front cover, the polymer

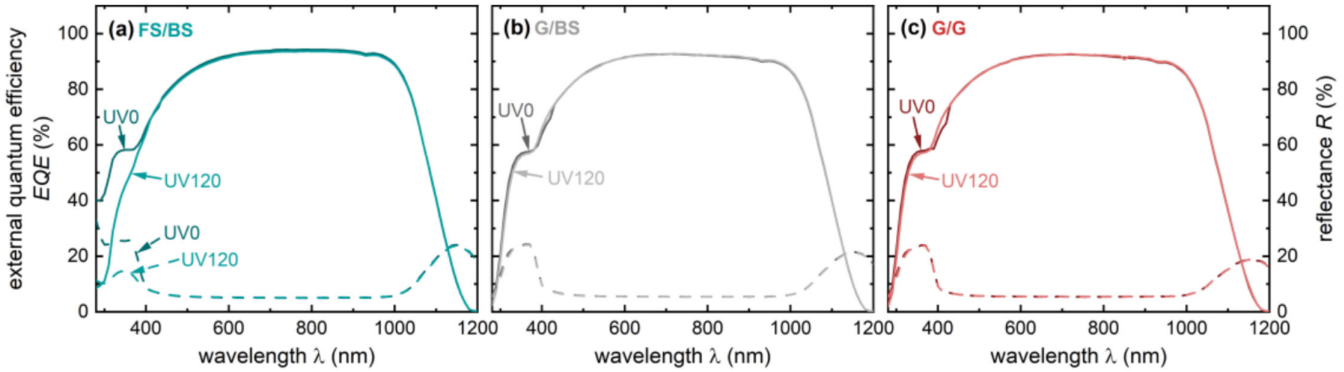

FIGURE 12 | *EQE* (solid line) and reflectance (dashed line) of solar modules using UV-DS encapsulants in different solar module structures: (a) front sheet/back sheet (FS/BS), (b) glass/back sheet (G/BS), and (c) glass/glass (G/G), measured before and after 120 kWh/m^2 of UV exposure.

front sheet in FS/BS solar modules provides less protection against oxidants, such as ozone and oxygen, facilitating their ingress and subsequent degradation of the downshifting particles. However, the chemical mechanism of this degradation requires further investigation.

Currently, the G/G and G/BS configurations dominate the PV market. This study demonstrates that the combination of downshifting encapsulants with these configurations yields high UV stability. In contrast, integrating downshifting encapsulants into lightweight solar module designs significantly reduces UV stability, highlighting the need for more reliable encapsulation strategies tailored to lightweight solar modules or more stable UV-downshifting materials.

3.3 | Dual-Layer Encapsulation Design: An Innovative Strategy to Enhance UV Utilization and Stability

3.3.1 | Advantages of the Dual-Layer Encapsulation Design

From the above analysis, the UV-DS encapsulant has been shown to shift UV photons into the visible range. However, residual UV photons, which are not shifted can still penetrate the encapsulant, inducing UVID in the solar cells. Furthermore, degradation of the DS effect was observed in lightweight solar modules with UV-DS encapsulant during UV exposure. As the DS effect deteriorates, an increasing fraction of UV photons remain unshifted, leading to greater passivation degradation, and consequently higher efficiency losses. To address this issue, a novel dual-layer encapsulant design was proposed, combining a UV-DS layer with a UV-B layer as the front encapsulant in lightweight solar modules. The structure of the solar module is illustrated in Figure 13. The configurations of the solar modules are shown in Table 1. CTM losses of lightweight SHJ solar modules with dual-layer encapsulants are shown in Figure S3. In this design, UV photons not effectively shifted by the UV-DS layer are subsequently blocked by the additional UV-blocking layer, thereby protecting the solar cells from UV-induced damage. A 120 kWh/m^2 of UV exposure was performed to assess the UV stability of this configuration.

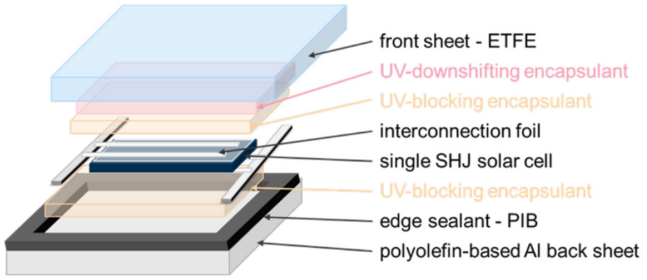

FIGURE 13 | Schematic of the lightweight SHJ single-cell solar module with dual-layer front encapsulant.

3.3.2 | Performance and Stability of Solar Modules With Dual-Layer Encapsulation Design

Figure 14 presents the evolution of normalized electrical parameters during UV exposure for the lightweight SHJ solar modules with the proposed dual-layer encapsulant design, compared with the single-layer UV-DS encapsulant design. Two dual-layer configurations were investigated: (i) UV-DS combined with UV-B$_{375}$ encapsulant and (ii) UV-DS combined with UV-B$_{350}$ encapsulant. The results show that both dual-layer designs exhibit lower efficiency degradation than the single-layer UV-DS module. Notably, the UV-DS + UV-B$_{375}$ module maintained η, *FF*, V_{oc}, and J_{sc} nearly unchanged after 120 kWh/m^2 of UV exposure, indicating excellent UV stability. In contrast, the UV-DS + UV-B$_{350}$ module displayed a slight efficiency reduction, primarily due to a decline in *FF*. This observation is consistent with the previous discussion that even a minimal number of UV photons in the 350–375-nm wavelength range can induce UVID in SHJ solar cells.

A comparison of PL imaging among the three solar module types is shown in Figure S4. The PL intensity of the UV-DS + UV-B encapsulant solar modules remained virtually unchanged after UV exposure, indicating stable passivation of the SHJ solar cells. In contrast, the UV-DS module exhibited a noticeable reduction in PL intensity, attributed to passivation degradation.

As previously discussed, *FF* losses are the primary cause of efficiency degradation in lightweight SHJ solar modules during UV exposure. Figure 15 shows the absolute changes in p*FF* and *FF*

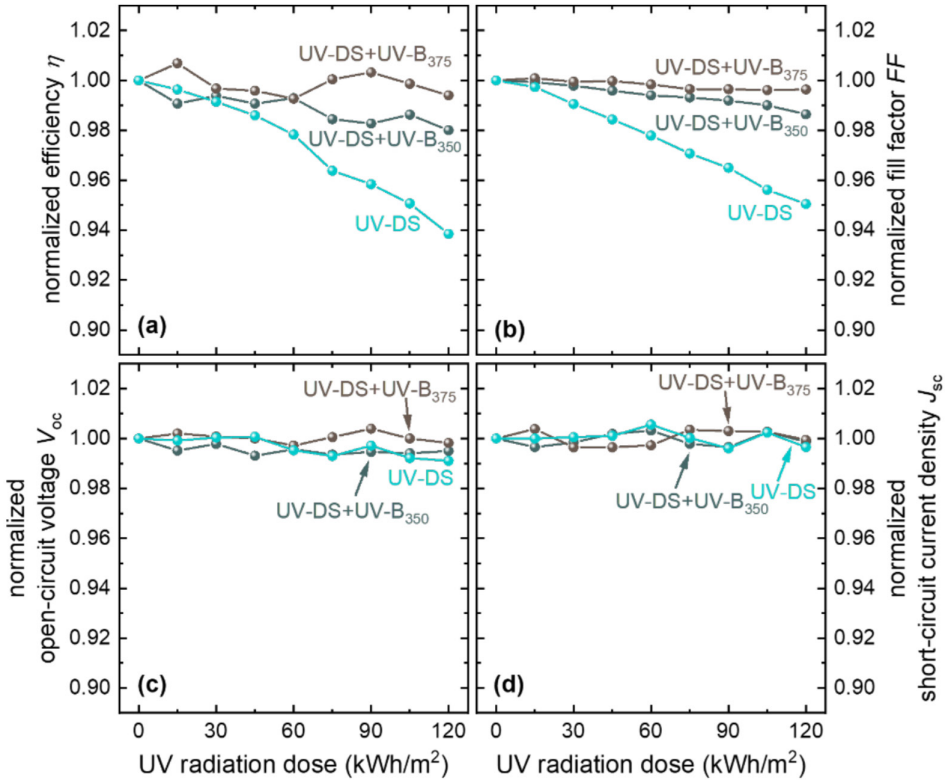

FIGURE 14 | Normalized values of (a) efficiency (η), (b) fill factor (*FF*), (c) open-circuit voltage (V_{oc}), and (d) short-circuit current density (J_{sc}) as a function of UV radiation dose for the lightweight SHJ solar modules with UV-DS, UV-DS + UV-B_{350}, or UV-DS + UV-B_{375} as the front encapsulant.

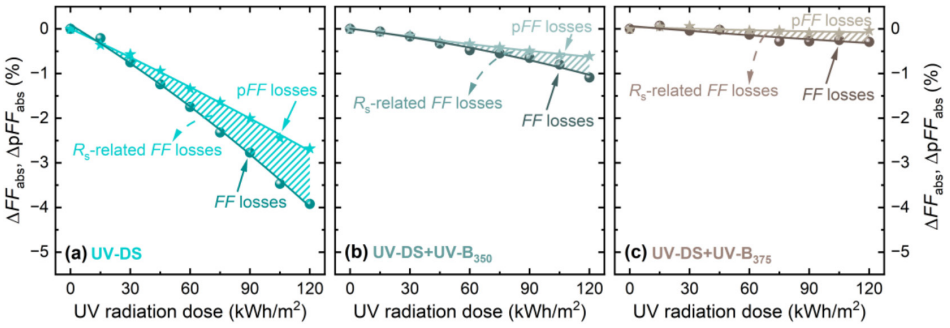

FIGURE 15 | Changes in pseudo fill factor (p*FF*) and fill factor (*FF*) of the lightweight SHJ solar modules with (a) UV-DS, (b) UV-DS + UV-B_{350} and (c) UV-DS + UV-B_{375}, as a function of UV radiation dose. ΔpFF_{abs} denotes the absolute change in p*FF*, whereas ΔFF_{abs} denotes the absolute change in *FF*.

for solar modules with dual-layer encapsulant and comparison to single-layer encapsulant. The dual-layer design (UV-DS + UV-B) exhibited smaller p*FF* and R_s-related *FF* losses than the single-layer (UV-DS) design. Notably, the p*FF* of the UV-DS + UV-B_{375} module remained stable, whereas the UV-DS + UV-B_{350} module showed a slight reduction in p*FF*. This minor decrease is attributed to the insufficient UV cutoff wavelength of the UV-B_{350} encapsulant, as discussed earlier.

Furthermore, the R_s-related *FF* losses were markedly reduced in the UV-DS + UV-B module, demonstrating that the novel dual-layer encapsulation design effectively suppressed R_s-related *FF* losses. As discussed in Section 3.2.2, the increase in R_s in lightweight solar modules is likely induced by moisture ingress, which deteriorates solar cell interconnections. The improved stability observed here can be attributed to the enhanced barrier properties of the dual-layer encapsulant, which more effectively hinders the ingress of moisture and oxidants compared with the single-layer design.

Figure 16 shows *EQE* and reflectance of the lightweight solar modules with the dual-layer encapsulant design, in comparison with those using a single-layer encapsulant, measured before and after 120 kWh/m^2 of UV exposure. *EQE* and reflectance of these lightweight solar modules exhibited a pronounced reduction in the short-wavelength range from (280–400 nm). The overall photocurrent loss derived from the *EQE* data was 0.90%$_{rel}$ for the UV-DS module, 0.85%$_{rel}$ for the UV-DS + UV-B_{350} module, and only 0.32%$_{rel}$ for the UV-DS + UV-B_{375} module. The latter effectively blocked most UV photons from reaching the

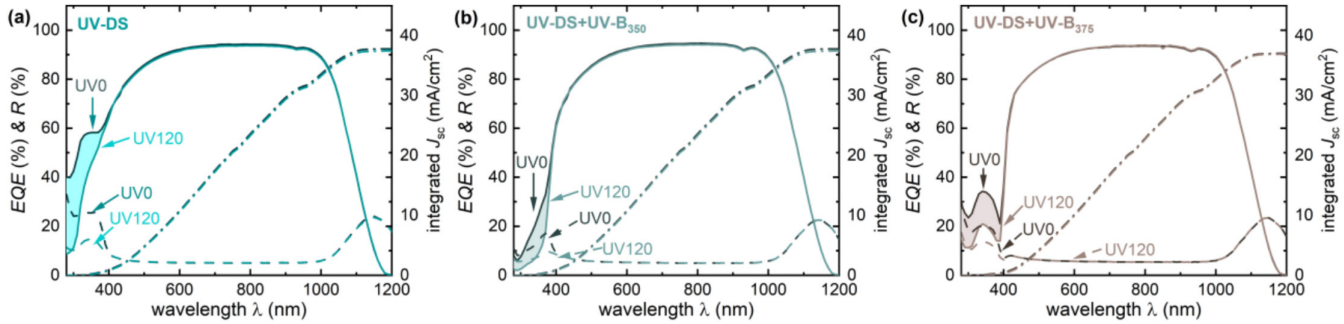

FIGURE 16 | *EQE* (solid line) and reflectance (dashed line) and integrated short-circuit current density (J_{sc}) (dashed dot line) of lightweight SHJ solar modules with (a) UV-DS, (b) UV-DS + UV-B_{350}, and (c) UV-DS + UV-B_{375}, measured before and after 120 kWh/m^2 of UV exposure.

solar cells, resulting in negligible p*FF* degradation and stable passivation properties, as indicated in Figure 15. Consequently, the observed *EQE* reduction in the UV-DS + UV-B_{375} module is attributed primarily to degradation of the DS effect, with the associated current loss limited to 0.32%$_{rel}$. Furthermore, the DS utilization efficiency, estimated from the *EQE* spectra, decreased from approximately 34% to 21% after 120 kWh/m^2 of UV exposure.

Although the DS effect degraded in all lightweight solar modules with DS encapsulants, the resulting photocurrent loss was limited to only 0.32%$_{rel}$. Incorporating a UV-B encapsulant in a dual-layer configuration with UV-DS significantly enhanced UV stability by reducing carrier recombination losses compared to a single-layer UV-DS design. As shown in Figure S5, the dual-layer solar module retained over 98% of its initial efficiency after 120 kWh/m^2 of UV exposure, representing an 8.92%$_{rel}$ higher post-exposure efficiency than the solar module with a UV-T encapsulant. This design not only delivers a higher initial power output but also maintains superior performance after UV exposure, indicating strong potential for improved long-term energy yield.

4 | Conclusions

This study comprehensively investigated the mechanism of UVID in lightweight SHJ solar modules utilizing UV-blocking, UV-transmitting, and UV-downshifting encapsulants. After 120 kWh/m^2 of indoor UV exposure, equivalent to 30 months of outdoor exposure in Jülich, Germany, solar modules incorporating these encapsulants exhibited relative efficiency losses of 2.17%, 9.25%, and 6.15%. The decrease in efficiency was mainly attributed to the decrease in V_{oc} and *FF* of the solar modules, accompanied by a diminished p*FF*. Accordingly, p*FF* loss was found to be the major cause of *FF* loss, which is attributed to the deterioration of the passivation properties of the solar cells due to UV radiation. Additionally, the influence of R_s-related *FF* losses increased, which is attributed to the deterioration of the interconnection foil supposedly caused by environmental factors such as moisture and oxygen, rather than UV radiation itself.

The results revealed that lightweight SHJ solar modules with UV-downshifting encapsulants effectively mitigated UVID. However, the UV-downshifting encapsulants cannot completely shift UV photons, and a reduction in the DS effect was observed, supposedly caused by the photooxidation. The chemical mechanism behind this requires further investigation. Utilization efficiency of DS decreases from around 34% to 21% after 120 kWh/m^2 of UV exposure. A novel encapsulation architecture combining UV-downshifting and UV-blocking encapsulants was proposed to ensure the UV utilization and stability of lightweight SHJ solar modules. Solar modules featuring this innovative dual-layer structure preserved over 98% of their initial performance after UV exposure, demonstrating a promising new approach for enhancing UV stability. The efficiency of this dual-layer solar module after UV exposure was 8.92%$_{rel}$ higher than that of the solar module with UV-transmitting encapsulant. The dual-layer structure provides more initial power, which remains high even after UV degradation, showing promising energy yield.

The comprehensive investigation provides substantial insights into the degradation mechanisms of lightweight SHJ solar modules under UV exposure and offers practical strategies in the progress of improving their durability and performance. In-depth investigation of the degradation mechanism of DS effect is still ongoing. The development of DS encapsulant foil with longer shifted wavelengths, such as green light, and higher reliability shows greater application potential.

Author Contributions

Kai Zhang, Andreas Lambertz, and Uwe Rau: study concept and design. **Kai Zhang and Rongda Zhang:** writing the original draft. **Rongda Zhang and Kai Zhang:** experimental testing and characterization. **Rongda Zhang, Kai Zhang, Karsten Bittkau, Andreas Lambertz, and Uwe Rau:** data analysis and interpretation. **Andreas Lambertz, Henrike Gattermann, Karsten Bittkau, Uwe Rau, and Kaining Ding:** review. **Andreas Lambertz and Uwe Rau:** study supervision.

Acknowledgements

The authors would like to thank Thomas Birrenbach, Christoph Zahren, Niklas Bongartz, and Volker Lauterbach for their technical assistance, and Dr. Timon Vaas for the PL measurement instruction. Rongda Zhang would like to thank Prof. Dr. Ruth Schwaiger for supervising his master's thesis. This work was supported by the Light.P.Roof project, which was funded by the Federal State North Rhine-Westphalia within the program "EFRE/JTF-Program NRW 2021-2027" under the grant number EFRE-20400082. Kai Zhang is grateful for the financial support from China Scholarship Council (No. 202108440128). Open Access funding enabled and organized by Projekt DEAL.

Conflicts of Interest

The authors declare no conflicts of interest.

Data Availability Statement

The data that support the findings of this study are available from the corresponding author upon reasonable request.

References

1. A. Descoeudres, C. Allebé, N. Badel, et al., "Silicon Heterojunction Solar Cells: Towards Low-Cost High-Efficiency Industrial Devices and Application to Low-Concentration PV," *Energy Procedia* 77 (2015): 508–514.

2. W. Duan, A. Lambertz, K. Bittkau, et al., "A Route Towards High-Efficiency Silicon Heterojunction Solar Cells," *Progress in Photovoltaics: Research and Applications* 30 (2021): 384–392.

3. H. Lin, M. Yang, X. Ru, et al., "Silicon Heterojunction Solar Cells With Up to 26.81% Efficiency Achieved by Electrically Optimized Nanocrystalline-Silicon Hole Contact Layers," *Nature Energy* 8 (2023): 789–799.

4. A. Louwen, W. van Sark, R. Schropp, and A. Faaij, "A Cost Roadmap for Silicon Heterojunction Solar Cells," *Solar Energy Materials & Solar Cells* 147 (2016): 295–314.

5. J. Haschke, O. Dupré, M. Boccard, and C. Ballif, "Silicon Heterojunction Solar Cells: Recent Technological Development and Practical Aspects—From Lab to Industry," *Solar Energy Materials & Solar Cells* 187 (2018): 140–153.

6. D. Qiu, W. Duan, A. Lambertz, et al., "Front Contact Optimization for Rear-Junction SHJ Solar Cells With Ultra-Thin N-Type Nanocrystalline Silicon Oxide," *Solar Energy Materials & Solar Cells* 209 (2020): 110471.

7. Y. Wang and D. Li, "Interfacial Fixed Charges and Dipoles to Boost Carrier Selectivity for Crystalline Silicon Solar Cells," *Innovation Energy* 1, no. 2 (2024): 100023.

8. Trinasolar, *Trinasolar Sets New N-Type Solar Cell Efficiency World Record of 27.08%* (Trinasolar, 2024), https://static.trinasolar.com/en-apac/resources/newsroom/aptrinasolar-sets-new-n-type-solar-cell-efficiency-world-record-27082024.

9. A. C. Martins, V. Chapuis, F. Sculati-Meillaud, A. Virtuani, and C. Ballif, "Light and Durable: Composite Structures for Building-Integrated Photovoltaic Modules," *Progress in Photovoltaics: Research and Applications* 26 (2018): 718–729.

10. A. C. Martins, V. Chapuis, A. Virtuani, and C. Ballif, "Robust Glass-Free Lightweight Photovoltaic Modules With Improved Resistance to Mechanical Loads and Impact," *IEEE Journal of Photovoltaics* 9 (2019): 245–251.

11. K. Zhang, O. Mashkov, A. Yaqin Muhammad, et al., "Damp-Heat–Induced Degradation of Lightweight Silicon Heterojunction Solar Modules With Different Transparent Conductive Oxide Layers," *Progress in Photovoltaics: Research and Applications* 33, no. 4 (2025): 541–550.

12. F. Lisco, F. Bukhari, L. O. Jones, A. M. Law, J. M. Walls, and C. Ballif, "ETFE and Its Role in the Fabrication of Lightweight c-Si Solar Modules," *IEEE Journal of Photovoltaics* 13 (2023): 349–354.

13. A. C. Martins, V. Chapuis, A. Virtuani, H.-Y. Li, L.-E. Perret-Aebi, and C. Ballif, "Thermo-Mechanical Stability of Lightweight Glass-Free Photovoltaic Modules Based on a Composite Substrate," *Solar Energy Materials & Solar Cells* 187 (2018): 82–90.

14. K. Zhang, A. Lambertz, K. Dzięcioł, et al., "Towards Integrated Photovoltaic Applications: Lightweight Silicon Heterojunction Solar Modules With Different Encapsulation Materials and Their Damp Heat Stability," *Applied Energy* 400 (2025): 126570.

15. J. Yu, Y. Bai, Q. Qiu, et al., "Reliability of Transparent Conductive Oxide in Ambient Acid and Implications for Silicon Solar Cells," *eScience* 4, no. 3 (2024): 100241.

16. O. Arriaga Arruti, A. Virtuani, and C. Ballif, "Long-Term Performance and Reliability of Silicon Heterojunction Solar Modules," *Progress in Photovoltaics: Research and Applications* 31 (2023): 664–677.

17. A. Sinha, J. Qian, S. L. Moffitt, et al., "UV-Induced Degradation of High-Efficiency Silicon PV Modules With Different Cell Architectures," *Progress in Photovoltaics: Research and Applications* 31 (2022): 36–51.

18. H. Ye, S. Huang, C. Qian, et al., "Short Wavelength Photons Destroying Si–H Bonds and Its Influence on High-Efficiency Silicon Solar Cells and Modules," *Solar RRL* 7 (2023): 7.

19. J. Ren, W. Zhao, J. Shi, et al., "Predicting the Lifetime of HJT Modules Towards the Outdoor Real-World Environment," *Solar Energy Materials & Solar Cells* 272 (2024): 112885.

20. B. Fischer, A. Lambertz, M. Nuys, et al., "Insights Into the Si Horizontal Line H Bonding Configuration at the Amorphous/Crystalline Silicon Interface of Silicon Heterojunction Solar Cells by Raman and FTIR Spectroscopy," *Advanced Materials* 35 (2023): e2306351.

21. G. Oreski, A. Omazic, G. C. Eder, et al., "Properties and Degradation Behaviour of Polyolefin Encapsulants for Photovoltaic Modules," *Progress in Photovoltaics: Research and Applications* 28 (2020): 1277–1288.

22. J. Morse, M. Thuis, D. Holsapple, R. Willis, M. D. Kempe, and D. C. Miller, "Degradation in Photovoltaic Encapsulant Transmittance: Results of the Second PVQAT TG5 Artificial Weathering Study," *Progress in Photovoltaics: Research and Applications* 30 (2022): 763–783.

23. M. C. C. d. Oliveira, A. S. A. Diniz Cardoso, M. M. Viana, and V. d. F. C. Lins, "The Causes and Effects of Degradation of Encapsulant Ethylene Vinyl Acetate Copolymer (EVA) in Crystalline Silicon Photovoltaic Modules: A Review," *Renewable and Sustainable Energy Reviews* 81 (2018): 2299–2317.

24. A. Ndiaye, A. Charki, A. Kobi, C. M. F. Kébé, P. A. Ndiaye, and V. Sambou, "Degradations of Silicon Photovoltaic Modules: A Literature Review," *Solar Energy* 96 (2013): 140–151.

25. M. Aghaei, A. Fairbrother, A. Gok, et al., "Review of Degradation and Failure Phenomena in Photovoltaic Modules," *Renewable and Sustainable Energy Reviews* 159 (2022): 112160.

26. K. R. McIntosh, N. E. Powell, A. W. Norris, J. N. Cotsell, and B. M. Ketola, "The Effect of Damp-Heat and UV Aging Tests on the Optical Properties of Silicone and EVA Encapsulants," *Progress in Photovoltaics: Research and Applications* 19 (2011): 294–300.

27. R. Witteck, B. Veith-Wolf, H. Schulte-Huxel, et al., "UV-Induced Degradation of PERC Solar Modules With UV-Transparent Encapsulation Materials," *Progress in Photovoltaics: Research and Applications* 25 (2017): 409–416.

28. B. Adothu, F. R. Costa, and S. Mallick, "UV Resilient Thermoplastic Polyolefin Encapsulant for Photovoltaic Module Encapsulation," *Polymer Degradation and Stability* 201 (2022): 109972.

29. H. Han, X. Dong, B. Li, et al., "Degradation Analysis of Crystalline Silicon Photovoltaic Modules Exposed Over 30 Years in Hot-Humid Climate in China," *Solar Energy* 170 (2018): 510–519.

30. Y. Chen, D. Chen, C. Liu, et al., "Mass Production of Industrial Tunnel Oxide Passivated Contacts (I-TOPCon) Silicon Solar Cells With Average Efficiency Over 23% and Modules Over 345 W," *Progress in Photovoltaics: Research and Applications* 27 (2019): 827–834.

31. S. Ma, D. X. Du, D. Ding, et al., "Improving the Performance of Industrial TOPCon Solar Cells Through the Insertion of Intrinsic a-Si Layer," *Solar Energy Materials & Solar Cells* 275 (2024): 113024.

32. C. Ballif, F.-J. Haug, M. Boccard, P. J. Verlinden, and G. Hahn, "Status and Perspectives of Crystalline Silicon Photovoltaics in Research and Industry," *Nature Reviews Materials* 7 (2022): 597–616.

33. F. T. Thome, P. Meßmer, S. Mack, et al., "UV-Induced Degradation of Industrial PERC, TOPCon, and HJT Solar Cells: The Next Big Reliability Challenge?," *Solar RRL* 8 (2024): 2400628.

34. Z. Yang, Y. Li, J. Wu, et al., "Novel EPE Co-Extruded Encapsulating Films With UV Down-Conversion Power Gain Effect for Highly Efficient Solar Cells," *Solar Energy Materials & Solar Cells* 257 (2023): 112373.

35. C.-K. Wu, S. Zou, C.-W. Peng, et al., "Improving the UV-Light Stability of Silicon Heterojunction Solar Cells Through Plasmon-Enhanced Luminescence Downshifting of YVO4:Eu3+,Bi3+ Nanophosphors Decorated With Ag Nanoparticles," *Journal of Energy Chemistry* 81 (2023): 212–220.

36. K. R. McIntosh, G. Lau, J. N. Cotsell, et al., "Increase in External Quantum Efficiency of Encapsulated Silicon Solar Cells From a Luminescent Down-Shifting Layer," *Progress in Photovoltaics: Research and Applications* 17 (2008): 191–197.

37. B. Xu, K. Bittkau, A. Eberst, et al., "Downshifting Encapsulant: Optical Simulation Evaluation of the Solution to Ultraviolet-Induced Degradation in Silicon Heterojunction Solar Cells," *Advanced Energy and Sustainability Research* 6 (2024): 2400227.

38. Deutscher Wetterdienst (DWD), 2008, https://www.dwd.de/DE/Home/home_node.html.

39. M. Koehl, M. Heck, and S. Wiesmeier, "Categorization of Weathering Stresses for Photovoltaic Modules," *Energy Science & Engineering* 6 (2018): 93–111.

40. J. Yang, Y. Tang, C. Zhou, et al., "Unveiling the Mechanism of Ultraviolet-Induced Degradation in Silicon Heterojunction Solar Cells," *Solar Energy Materials & Solar Cells* 276 (2024): 113062.

41. S. V. Spataru, D. Sera, P. Hacke, T. Kerekes, and R. Teodorescu, "Fault Identification in Crystalline Silicon PV Modules by Complementary Analysis of the Light and Dark Current–Voltage Characteristics," *Progress in Photovoltaics: Research and Applications* 24 (2015): 517–532.

42. P. Würfel, *Physics of Solar Cells From Principles to New Concepts* (Wiley-VCH Verlag GmbH & Co. KGaA, 2005).

43. K. Vandewal, K. Tvingstedt, A. Gadisa, O. Inganas, and J. V. Manca, "On the Origin of the Open-Circuit Voltage of Polymer-Fullerene Solar Cells," *Nature Materials* 8 (2009): 904–909.

44. N. C. Park, J. S. Jeong, B. J. Kang, and D. H. Kim, "The Effect of Encapsulant Discoloration and Delamination on the Electrical Characteristics of Photovoltaic Module," *Microelectronics and Reliability* 53 (2013): 1818–1822.

Supporting Information

Additional supporting information can be found online in the Supporting Information section. **Figure S1:** Transmittance (solid line, *T*) and reflectance (dashed line, *R*) spectra of different encapsulants: (a) TPO (UV-B_{350}), (b) PO (UV-B_{375}), (c) EVA (UV-T), measured by UV–vis–NIR spectrophotometer, before and after 120 kWh/m^2 of UV exposure. (d) Transmittance of DS-EVA (UV-DS) before, after 60 kWh/m^2, and after 120 kWh/m^2 of UV exposure, measured by an in-house-built setup. (e) Transmittance (solid line, *T*) and reflectance (dashed line, *R*) of ETFE front sheet measured by UV–vis–NIR spectrophotometer, before and after 120 kWh/m^2 of UV exposure. (f) Comparison of transmittance (solid line, *T*) and reflectance (dashed line, *R*) of ETFE front sheet with glass. **Figure S2:** Excitation and emission spectra of downshifting encapsulant foil. **Figure S3:** CTM loss from (a) efficiency (η), (b) fill factor (*FF*), (c) short-circuit current density (J_{sc}), and (d) series resistance (R_s) of lightweight SHJ solar modules incorporating encapsulants with different UV-transmission properties. C stands for solar cell and M stands for solar module. **Figure S4:** PL images of lightweight SHJ solar modules with (a) UV-DS, (b) UV-DS + UV-B_{350}, and (c) UV-DS + UV-B_{375}, measured before and after 120 kWh/m^2 of UV exposure. **Figure S5:** Solar module efficiency before and after 120 kWh/m^2 of UV exposure, with currents for efficiency calculation derived from *EQE* measurements. **Table S1:** Specifications of encapsulants. **Table S2:** Specifications of front sheet and back sheet.